

Biological iron-sulfur clusters: mechanistic insights from mass spectrometry

Jason C. Crack and Nick E Le Brun*

*Address correspondence to: Nick E Le Brun, School of Chemistry, University of East Anglia, Norwich Research Park, Norwich NR4 7TJ, UK. Tel. +44 1603 592699; Fax. +44 1603 592003; Email: n.le-brun@uea.ac.uk.

Highlights

- Iron-sulfur clusters are ubiquitous in life and diverse in function
- Native mass spectrometry provides novel insight into iron-sulfur cluster chemistry
- Cluster-specific Fe/S isotope substitutions confirm mass spectrometric assignments
- Time-resolved native mass spectrometry unravels mechanisms of cluster conversion

Abstract

Iron-sulfur (FeS) clusters are protein cofactors that are ubiquitous in life, performing a wide range of functions, such as in electron transfer, catalysis and gene regulation. This functional diversity is underpinned by the inherent reactivity of FeS clusters towards redox change and reaction with small molecules such as molecular oxygen and nitric oxide. Such reactivity also presents significant challenges for their study, and difficulties in obtaining sufficient quantities of stable, homogenous FeS protein samples have severely hampered progress in understanding these fascinating proteins. Recently, the application of mass spectrometry, under conditions where the cluster cofactor remains protein-associated, has yielded major new insight, particularly into FeS cluster assembly and the chemistry occurring at the FeS clusters of transcriptional regulators that coordinate the cell's response to changing conditions, such as availability of O₂ and cellular iron status, or the onset of oxidative or nitrosative stress. Here we review this recent progress, highlighting the power of native mass spectrometric approaches for studies of protein cofactors.

Keywords: iron-sulfur cluster, mass spectrometry, DNA regulation, iron-sulfur cluster biogenesis, iron sensing, oxygen sensing, nitric oxide sensing.

Abbreviations: Cys, cysteine; DNIC, dinitrosyl iron complex; DPTA, dipropylenetriamine; EDTA, ethylenediaminetetraacetate; EPR, electron paramagnetic spectroscopy; ESI-TOF, electrospray ionization – Time of flight; IRO, iron responsive operator; FeS, iron-sulfur; His, histidine; K_d , dissociation constant; LC-MS, liquid chromatography mass spectrometry; NO, Nitric oxide; NRVS, nuclear resonance vibrational spectroscopy; PLP: pyridoxal 5' phosphate; RBS, Roussin's black salt; RRE, Roussin's red ester.

1. Introduction

It is estimated that between a third and a half of all proteins utilise a metal ion (from alkaline and alkaline earth to transition metals) for catalytic function or structural stability. In terms of abundance and functional diversity, iron is perhaps the most prevalent metal ion in biology [1, 2]. Iron-containing proteins can be broadly separated into distinct types, depending on the nature of the iron cofactor: heme, non-heme iron and iron-sulfur proteins. Heme proteins contain iron coordinated at the centre of a porphyrin macrocycle. Non-heme iron proteins contain one or more irons coordinated directly by protein amino acid residues. Iron-sulfur proteins contain a cluster of multinuclear iron and inorganic sulfide, where the irons are coordinated by protein amino acid residues and sulfides [3-8].

Iron-sulfur (FeS) cluster-containing proteins are present in virtually all forms of life and are involved in a diverse range of cellular processes (e.g. respiration, photosynthesis, central metabolism, DNA metabolism, and gene regulation). They can be grouped broadly according to whether they function in electron transfer, catalysis, structural stability, or as sensors; in many cases, their redox properties are a central feature of their functional role(s) [9-13]. The simplest FeS cluster is the [2Fe-2S] cluster, which consists of a $[\text{Fe}_2(\mu_2\text{-S})_2]$ rhomb, with each iron coordinated by two further amino acid side chains from the protein scaffold. These residues are usually cysteine thiolates (RS^-), but other residues, most notably serine (RO^-), histidine ($-\text{N}=\text{}$), aspartate or glutamate (RCOO^-), are sometimes found, particularly for clusters associated with catalysis or sensing functions [5, 14-16], see Fig. 1. Because each iron is tetrahedrally coordinated, the four protein ligands are constrained to lie in a plane perpendicular to that of the $[\text{Fe}_2(\mu_2\text{-S})_2]$ rhomb (Fig. 1).

The [4Fe-4S] cluster may be thought of as comprising two $[\text{Fe}_2(\mu_2\text{-S})_2]$ rhombs, one on top of the other at right angles to each other, generating a cuboidal arrangement. In this case, each iron is coordinated by only one amino acid side chain, which, again, is most commonly cysteine, with the coordinating side chains positioned at the vertices of the cluster cube (Fig. 1). Removal of one iron from a [4Fe-4S] cluster generates a [3Fe-4S] cluster. Other, less common arrangements include naturally occurring hetero-metal clusters (e.g. $[\text{Mo-3Fe-4S}]$), and the unusually coordinated $[\text{4Fe-3S}](\text{Cys})_6$ cluster [17, 18] (Fig. 1).

The oxidation state of each iron is invariably +2 or +3 and, because of the tetrahedral coordination, is always high spin having either four or five unpaired electrons respectively. Electron delocalization and spin coupling between different iron ions results in no, or a minimum of, unpaired electrons (reviewed in [19, 20]). The current picture of accessible core oxidation states, valence delocalization schemes and resultant spin states for commonly encountered FeS clusters has been reviewed elsewhere [5-9]. Although each cluster may adopt several different charge states, the biological role of the protein normally confines the cluster to a pair of oxidation states, e.g. the +2/+1 couple is most common among electron transfer proteins [5].

FeS clusters are also susceptible to damage from reactive oxygen species, including molecular oxygen, superoxide ion and hydrogen peroxide [21]. This can lead to partial or total loss of the cluster, or trigger a cluster interconversion. Reactions with strongly coordinating species such as nitric oxide (NO), or other cellular components, can also lead to cluster damage/conversion. In the case of association with NO, coordination is accompanied by redox processes. While this inherent sensitivity to a range of potentially biologically important species means that FeS cluster proteins are often amongst the first to be inactivated when cells are subjected to stress conditions, it has also been exploited during evolution through the incorporation of FeS clusters as the sensory modules of some transcriptional regulators.

Current understanding of FeS cluster proteins has resulted from the application of a very wide range of techniques and methods, including: multiple spectroscopies, such as absorbance, circular dichroism, magnetic circular dichroism [22], electron paramagnetic resonance (EPR) [23, 24], Mössbauer [25, 26] and resonance Raman [27]; structural methods such as X-ray crystallography [15, 28] and NMR [29]; electrochemistry [5-8, 30, 31]; and theoretical/computational methods [19, 32-34]. In general, the application of complementary techniques has led to the greatest insight. A limitation of the methods traditionally applied in studies of FeS cluster proteins is that none of them can simultaneously distinguish multiple closely related FeS species, such as the intermediates in a FeS cluster conversion reaction. Therefore, methods that can provide novel and complementary information are continuously sought.

Mass spectrometry (MS) is an indispensable tool for biological research, owing to its capacity to identify and quantify proteins and other cellular components in complex mixtures. The interfacing of reversed phase liquid chromatography (LC) with electrospray ionization (ESI) to enable on-line MS detection has remained the default approach to proteomics for many years. FeS clusters, which are acid labile, along with non-covalent protein-protein or protein-cofactor interactions, are lost under the mildly acidic conditions of LCMS. In the early 1990s, the detection of non-covalently bound protein cofactors suggested it was possible to ionize macromolecules by ESI under conditions where non-covalent interactions are preserved, and thus gain high resolution mass information on protein-associated complexes [35-39] (for a contemporary review, see [40]).

Today, with advancements in instrument hardware, even a modest benchtop ESI quadrupole-time-of-flight (Q-TOF) instrument offers good resolution, while higher specification Q-TOF instruments capable of measurements over extended m/z ranges, quadrupole-Orbitrap, and Fourier transformed ion cyclotron resonance (FTICR) spectrometers offer increasing (in that order) resolution and sensitivity. Newer mass spectrometer configurations now incorporate ion mobility methodologies for the enhanced separation of closely related species and access to molecular shape/architecture information, in addition to mass [41].

Applications of non-denaturing MS, often referred to as native MS, are increasingly being used to investigate non-covalently bound protein cofactors, simple protein-protein complexes, or multi-protein super complexes [42, 43]. Amongst studies of protein-cofactor interactions are an increasing number on proteins that contain metallo-cofactors [2, 44-59]. These have been particularly insightful where there is chemistry taking place at the cofactor, owing to the unique capability of native MS to simultaneously measure the accurate mass of multiple species, which may be different forms of the same protein, present in solution. The ability of MS to resolve different isotopes of metallo-cofactors has also been exploited to assist with unambiguous assignments [60].

Prior to performing native mass spectrometry of FeS proteins, all non-volatile salts (e.g. NaCl, KCl, phosphate etc.) and buffer components (Tris, HEPES, MES, etc.) must be removed from the protein sample and replaced with volatile buffer components. This is usually carried out by exchanging samples into solutions of ammonium acetate under an inert atmosphere (e.g. nitrogen). In some cases, ammonium acetate may ligate iron, triggering cluster disassembly. If this is suspected, ammonium formate, ammonium bicarbonate or triethyl ammonium bicarbonate may be used (for further details see [43, 61, 62]). Proteins may be introduced into the spectrometer by direct infusion, or via native LC methods utilizing size exclusion or ion exchange chromatography [63].

In native MS, the partial dissociation of proteins that are dimeric in solution into monomers is a well-known phenomenon, and arises due to a number of causes, including the

application of excess energy following transfer to the gas phase (collisional activation), and the disruption of hydrophobic interactions that stabilise the dimer during transfer to the gas phase [64-66]. Irrespective of origin, this has proved to be advantageous for studies involving FeS proteins because it simplifies the identification of FeS species, which could potentially be different in the two subunits of a dimeric FeS protein.

During analysis masses are derived from the recorded m/z spectra according to $[M + zH]/z$, where M is the molecular mass of the protein, H is the mass of the proton and z is the charge of the ion. However, additional considerations are required for the analysis of metalloproteins, since metal cofactors typically carry charge, which must be considered. For FeS proteins, the peaks correspond to $[M + [FeS]^x + (z - x)H]/z$, where M is the molecular mass of the protein, $[FeS]^x$ is the mass of the FeS cluster with x charge, H is the mass of the proton and z is the charge of the ion. In this expression the charge of the cluster, x , offsets the number of protons required to obtain an ion with z charge. Post deconvolution, the observed mass is usually off-set from the predicted mass by the charge of the cluster, $[M + ([FeS]^x - x)]$. For example, a protein of mass M that binds a $[4Fe-4S]^{2+}$ cluster gives rise to a corresponding peak (M^{obs}) for the holo-protein according to $M^{obs} = (M + (352 - 2))$ Da [57, 67, 68]. This is a consequence of charge-compensation, where binding of a charged cofactor normally results in dissociation of protons such that overall charge balance is maintained. We refer readers interested in practical considerations concerning native MS measurements of FeS cluster proteins, including sample preparation, instrument parameters and data interpretation to a recent review [61].

Here we review the recent use of native MS as a method to gain unprecedented insights into FeS cluster proteins, with a focus is on FeS cluster biogenesis and analyte-sensing mechanisms employed by FeS cluster containing transcriptional regulators, which provide the most powerful illustrations to date of native MS applications to FeS proteins.

2. Iron-sulfur cluster biogenesis

Iron-sulfur (FeS) clusters spontaneously assembly *in vitro* under anaerobic conditions if sulfide (S^{2-}) and $Fe^{2+/3+}$ ions are combined with apo-protein in the presence of a thiol-based reductant [10, 69, 70]. In contrast, living organisms require multiprotein machineries that *de novo* synthesize the FeS cluster on a dedicated scaffold protein (e.g. IscU, reviewed in [71, 72]), enabling the coordinated availability of the potentially highly toxic iron and sulfide. Three FeS assembly systems, named Isc, Suf, and Nif, are found in bacteria. The *isc* operon (*iscRSUA-hscBA-fdx-iscX*) of *E. coli* is perhaps the best understood of these, with an overall mechanism having been elucidated two decades ago, see [72]. A related FeS cluster (ISC) biosynthetic pathway is also found in the mitochondria of eukaryotes [73]. Regulation of FeS cluster homeostasis in *E. coli* is mediated at the transcriptional level by the IscR transcriptional regulator (discussed briefly in section 3; see [74]). Crystal structures of the sulfide-generating cysteine desulfurase IscS, alone and in complex with the scaffold protein IscU, have been reported (PDB 3LVM, 3LVL) [75]. Structures of apo- and $[2Fe-2S]$ IscU (PDB 2L4X, 2Z7E) have provided key insights into the mechanism of intramolecular sulfur transfer and associated protein-protein interactions [76-78], see Fig. 2a. IscS exists as obligate homo-dimer with one pyridoxal 5' phosphate (PLP) cofactor bound per monomer. In the presence of IscU, an $(IscS)_2(IscU)_2$ complex is obtained [75].

Using native MS, Puglisi *et al* [52] and Lin *et al* [53] were able to detect PLP-containing IscS dimers. The inclusion of IscU gave an $(IscU)_2(IscS)_2$, consistent with previous solution and crystallographic observations. Both groups also observed an $(IscU)(IscS)_2$ species,

suggesting a dynamic equilibrium exists in solution between $(\text{IscS})_2$, IscU and the $(\text{IscU})_2(\text{IscS})_2$ complex [52, 53] (Fig. 2b). *In vivo and in vitro*, IscU exists in two distinct forms that are in equilibrium: a structured (S-) and dynamically disordered (D-) states [79-81]. Both Puglisi *et al* and Lin *et al* found S- and D-states of IscU to be monomeric, with a minor dimeric S-state component [52, 53]. Lin *et al* further demonstrated that IscU readily dimerized under aerobic conditions, even in the presence of glutathione, due to the formation of an intermolecular disulfide bond (RS-SR) between cysteine residues of the FeS cluster assembly site [53].

The binding of hexaqua Fe to IscU has been studied in solution for both eukaryotic and prokaryotic homologues. These studies have shown that IscU contains a primary, high affinity Fe^{2+} site ($K_d \sim 3 \mu\text{M}$) in addition to a secondary lower affinity site ($K_d \sim 25 \mu\text{M}$) [82-84]. We note that the concentration of 'free' (cheatable) iron in the *Escherichia coli* cytoplasm is $\sim 10 \mu\text{M}$ [85]

Native MS of as isolated IscU revealed the presence of one Zn^{2+} ion per monomer, as previously reported (PDB 1Q48) [53, 86]. While Zn^{2+} has been shown to stabilise the structured S-state of IscU , excess intracellular Zn^{2+} disrupts FeS assembly and inhibits growth in *E. coli* [87, 88]. Through additional native MS experiments, it was found that Zn-IscU is less prone to RS-SR induced dimer formation. Zn-IscU is also resistant to displacement by Fe^{2+} ions (with IscU alone or associated with IscS) or physiologically relevant low molecular weight thiols (e.g. L-Cys, GSH), and exhibits lower [2Fe-2S] cluster formation activity with catalytic quantities of IscS . In contrast, the Zn^{2+} ion could be removed in the presence of equimolar amounts of Zn-IscU and IscS with excess Cys [53]. Zn-IscU readily forms $(\text{IscU})_2(\text{IscS})_2$ and $(\text{IscU})(\text{IscS})_2$ quaternary structures, suggesting Zn removal by IscS may be linked to the catalytic function of IscS and thus physiologically relevant [53]. *In vitro*, the high affinity chelator diethylenetriaminopentaacetic acid (DTPA) can be used to remove Zn^{2+} ion from Zn-IscU , to give apo- IscU , while control experiments suggested that native MS faithfully reflected relative concentrations of species known to be in solution [53].

Titration of apo- IscU samples containing a mixture of monomeric and dimeric apo- IscU , in addition to some Zn-IscU , with Fe^{2+} ions revealed that apo- IscU binds a single Fe^{2+} ion at low Fe^{2+} concentrations, followed by a second Fe^{2+} at higher concentrations (≥ 20 fold molar excess), consistent with the primary and secondary binding sites elucidated from solution studies. When associated with IscS , two Fe^{2+} ions (2-fold molar excess) were observed to bind to the $(\text{IscU})_2(\text{IscS})_2$ species, presumably at the primary, high affinity, site identified by solution studies [53, 82-84]. We note that at low concentrations of Fe^{2+} (≤ 20 -fold molar dimeric excess) dimeric IscU failed to acquire Fe^{2+} ions, suggesting the thiols involved in the intermolecular disulfide bonds form part of the primary, high affinity, iron binding site [53]. Studies of mitochondrial ISC FeS cluster assembly, employing LC-MS amongst other methods, revealed that Fe^{2+} -binding to IscU activated the transfer of persulfide from NFS1 to IscU , facilitating its reduction by ferredoxin FDX2 to sulfide [55].

Native MS can also be used to probe the formation of intermediates species in a time resolved manner, and so has the potential to report on the precise sequence of events leading to the assembly of an FeS cluster by the Isc system. Lin *et al* followed the formation of intermediates on monomeric IscU (generated by in source disassociation of the $(\text{IscU})_2(\text{IscS})_2$ complex) during FeS assembly. Within the first few minutes of the reaction time course, $[\text{Fe}]$ -, $[\text{Fe}_2]$ -, $[\text{FeS}]$ -, $[\text{S}]$ and $[\text{S}_2]$ forms of IscU rapidly increased in concentration, and subsequently declined as the product, [2Fe-2S] IscU , was formed, leading to the proposal of an 'iron first mechanism' [53], see Fig. 2c.

Two additional Fe binding proteins, CyaY and IscX, have overlapping binding sites on dimeric IscS. CyaY, a frataxin homologue, was initially proposed to be the Fe donor for the *isc* system, but was subsequently shown to inhibit FeS biogenesis under certain conditions in prokaryotes [89], leading to the proposal that CyaY functions in the regulation of FeS biogenesis activity. Recent native MS data showed that (IscS)₂ has a preference for apo-CyaY, over Fe-CyaY, with (CyaY)(IscS)₂ and (CyaY)₂(IscS)₂ complexes being observed. CyaY also formed complexes with IscU and (IscU)_{n=1,2}(IscS)₂ [52]. A direct interaction between IscU and CyaY is consistent with solution studies of the eukaryotic homologue. In comparison to CyaY, IscX has a lower affinity for iron and a higher affinity for IscS [52]. As reported by Adinolfi *et al* [89], the inclusion of IscX in solutions of IscS resulted in (IscX)(IscS)₂ and (IscX)₂(IscS)₂ quaternary structures at stoichiometric ratios, with (IscX)₄(IscS)₂ being observed at higher IscX:IscS ratios. The affinity of IscX for IscS did not change significantly in the presence of IscU. These and other data suggest that IscX modulates the inhibitory properties of CyaY by competing for the same binding site on IscS, and that this effect is stronger at low iron concentrations, and negligible at higher iron concentrations [89].

Protein-protein interactions are likewise key to human FeS cluster biogenesis. Native MS was recently employed to investigate the post-assembly process of FeS cluster trafficking, providing evidence for [2Fe–2S]-cluster-bridged homodimeric glutaredoxin 5 (GLRX5), and a GLRX5:BoLA-like protein 3 (BOLA3) heterodimer. Furthermore, with recipient a ferredoxin (FDX2), transient cluster-transfer intermediates, such as (FDX2:GLRX5:[2Fe-2S]:GSH), were also revealed [54], yielding important new insight on trafficking pathways.

Overall, the studies highlighted here show how MS and particularly native MS is now being applied as a powerful tool to provide unprecedented details of protein-protein, protein ligand and even the time-dependent tracking of reaction intermediates involved in FeS cluster assembly.

3. FeS clusters as sensors of iron

In *E.coli*, IscR, encoded by the first gene of the *isc* operon, is the master regulator of FeS cluster biogenesis, controlling the transcription of both the *isc* and *suf* operons, and in doing so maintains FeS cluster homeostasis under both normal and stress conditions [74]. IscR belongs to the Rrf2 superfamily of transcriptional regulators that can be broadly divided according to whether or not they contain an FeS cluster [90, 91]. The [2Fe-2S] cluster utilised by IscR is very likely coordinated by an atypical (Cys)₃(His) motif, which may make IscR a less efficient client for the Isc machinery compared to other protein clients [16, 74, 90]. Additional factors, including iron limitation and oxidative stress, also play a role modulating the expression of FeS biogenesis systems in *E. coli* (see [74]).

In *Rhizobium leguminosarum*, the rhizobial iron regulator (RirA) shares ~48% homology with IscR and has been shown to repress many genes involved in iron uptake and homeostasis, as well as genes involved in FeS cluster biosynthesis, by binding to an iron responsive operator (IRO) sequence located upstream of RirA controlled genes (e.g. *fhuA*). In some species, including *R. leguminosarum*, RirA functions alongside a second global iron responsive transcriptional regulator, Irr, a member of the Fur family [92-95]. Unlike other Fur-like proteins, Irr appears to sense the presence of iron indirectly through the binding of heme [96]. These observations led to the hypothesis that RirA, like IscR, may sense iron via an FeS cluster [92].

As yet, there is no high resolution structure available for RirA, but a model based on its similarity to other Rrf2 family regulators is available (Fig. 3a). Anaerobic preparations of

RirA revealed the presence of a stable [4Fe-4S] cluster (*in vivo* or *in vitro* assembled) that binds tightly ($K_d \sim 170$ nM) to the IRO containing promoter region of *fhuA*. In contrast, apo-RirA exhibited a much lower affinity ($K_d > 5$ μ M) for the *fhuA* promoter [93]. In response to low iron conditions (induced by the iron chelator EDTA) or molecular oxygen, optical spectra revealed a pronounced red shift, followed by a gradual loss of absorption intensity throughout the visible region (>380 nm), indicative of the formation of a [2Fe-2S] cluster prior to cluster loss and the appearance of apo-RirA. The lack of dependence on the concentration or type of chelator suggested that the process may involve dissociation of iron from the cluster and its subsequent binding by the chelator. The conversion process could be followed by electron paramagnetic resonance (EPR) spectroscopy, and was found to involve the formation of a transiently stable [3Fe-4S]¹⁺, while the combination of anaerobic gel filtration and EPR further hinted at the presence of a [4Fe-4S]²⁺ \leftrightarrow [3Fe-4S]¹⁺ + Fe²⁺ equilibrium. Additional DNA binding experiments with the [2Fe-2S] form of RirA showed binding to the *fhuA* promoter, but with a significantly weaker affinity ($K_d \sim 482$ nM) [93]. The presence of residual [4Fe-4S] RirA might have contributed to the observed binding, and we note that the transiently stable [3Fe-4S]¹⁺ RirA may also be competent for DNA binding, as reported for the *Dinoroseobacter shibae* homologue [97].

Many transcriptional regulators exist as homodimers, stabilised by hydrophobic interactions [15, 28, 91, 98]. During native MS these hydrophobic interactions can become disrupted upon transfer to the gas phase [64]. Whilst artificial, it reduces sample complexity and greatly assists data interpretation. The native MS spectrum of RirA, measured in the monomeric region, was dominated by a peak at 17,792 Da, consistent with [4Fe-4S] RirA. Minor, well resolved peaks were observed on the low mass side, corresponding to traces of RirA containing [4Fe-3S], [3Fe-4S], [3Fe-3S], [3Fe-2S] and [2Fe-2S] clusters (Fig. 3b). In the dimer region, a dominant peak at 35,585 Da corresponding to [4Fe-4S] RirA homodimer was observed. A secondary peak on the low mass side corresponded to a dimer containing both [3Fe-4S] and [4Fe-4S] clusters [99]. The observation of a [3Fe-4S] cluster following sample preparation for native MS, which involves desalting (gel filtration), was consistent with EPR observations [93, 99].

To further establish the nature of cluster conversion process, [4Fe-4S] RirA was analysed by native MS under anaerobic low iron conditions (induced by EDTA). After 30 min, the monomeric region featured two peaks at 17,550 and 17,615 Da, corresponding to the presence of [2Fe] and [2Fe-2S] RirA (Fig. 3b). As expected from optical spectroscopy, the peak due to [4Fe-4S] RirA, along with other cluster breakdown species, were at a low abundance ($\leq 20\%$) relative to [2Fe-2S] RirA. In the dimer region, RirA homodimers containing [2Fe-2S] and [4Fe-4S] clusters were observed, in addition to dimers containing [3Fe-4S]/[4Fe-4S], [3Fe-4S]/[3Fe-4S], [3Fe-3S]/[3Fe-3S] and [2Fe-3S]/[3Fe-3S], consistent with conversion of [4Fe-4S] into [2Fe-2S] clusters over this time period [99].

The rate of the RirA cluster conversion suggested it might be possible to follow the iron-responsive cluster conversion process using native MS in real time [93, 99]. The peak due to monomeric [4Fe-4S] RirA gradually decayed away during the time course of the reaction. Additional peaks corresponding to protein bound cluster fragments, including [4Fe-3S], [3Fe-4S], [3Fe-3S], [3Fe-S], [2Fe-2S] and [2Fe-2S] (17,856 – 17,762 Da) initially increased in intensity before decaying away to apo-RirA at later time points (Fig. 3b and c). Data were fitted using the program Dynafit in order to generate a mechanistic model [100]. The data showed that the [4Fe-3S] and [3Fe-4S] clusters were the first intermediates to reach their maximum abundance, consistent with them being early intermediates in the conversion process, and the temporal appearance of [3Fe-4S]¹⁺ cluster by EPR. The [3Fe-3S] species

was the next intermediate to maximise, followed by the [3Fe-2S] species. The last intermediate to maximize in abundance was [2Fe-2S] RirA (Fig. 3c).

An equivalent study in the presence of O₂ showed that the same set of cluster intermediates was observed, but several steps of the cluster conversion process/degradation occurred at an enhanced rate, and the oxidation state of the [3Fe-4S]^{0/1+} cluster (which could be monitored by EPR) was also affected [93, 99]. Importantly, however, the initial reversible step in which the cluster loses a Fe²⁺ ion to form the [3Fe-4S]⁰ intermediate was not affected by the presence of O₂, consistent with this step, [4Fe-4S]²⁺ ⇌ [3Fe-4S]^{0/1+} + Fe²⁺, being the key iron-sensing reaction: under low iron conditions, the [3Fe-4S]⁰ cluster accumulates but is unstable, resulting in de-repression of RirA-regulated genes. Consistent with this, the affinity of Fe²⁺ for the [3Fe-4S]⁰ cluster was found to be in the expected physiological range ~(*K*_d = 3 μM) [99]. The susceptibility of the intermediate [3Fe-4S]⁰ cluster to oxidation to [3Fe-4S]¹⁺ is proposed as the mechanism of O₂-sensing, such that cluster conversion/degradation occurs more rapidly in the presence of O₂ than under anaerobic conditions (Fig. 3d). For a more detailed discussion, see [99]. We note that a similar native MS approach was used to study the Zn²⁺ sensor SmtB, which functions as a repressor in its apo-form, demonstrating that the major form of Zn²⁺-bound SmtB is the (SmtB)₂(Zn²⁺)₄ species, with both high affinity and sensory sites occupied [62].

Time resolved native MS was also used to follow cluster degradation in the RirA dimer itself. The major species prior to the addition of EDTA were [4Fe-4S]/[4Fe-4S] and [3Fe-4S]/[4Fe-4S] forms. Post addition, dimers containing [3Fe-4S]/[3Fe-4S] and [2Fe-2S]/[2Fe-2S] were readily observed. We note that for data relating to the dimer, the presence of two clusters in many cases precludes the unambiguous identification of intermediates because there are many more possible permutations as each of the two clusters undergoes conversion/degradation [99]. Nevertheless, the temporal behaviour of tentatively assigned dimeric species could be fitted to a basic model of cluster conversion based on the more detailed analyses of RirA monomer data [99].

For iron-sulfur proteins, using ³⁴S-, ⁵⁷Fe- or ³⁴S/⁵⁷Fe-substituted forms is often crucial for providing unambiguous confirmation of peak assignments for cluster conversion intermediates and products, and allows differentiation between them and any unrelated background adducts. Techniques for the production, isolation and analysis of ³⁴S-, ⁵⁷Fe- or ³⁴S/⁵⁷Fe-substituted iron-sulfur proteins have been described [68, 99, 101, 102].

4. FeS clusters as sensors of nitric oxide

The nitrite sensitive repressor (NsrR), first described in the ammonia oxidizing bacterium *Nitrosomonas europaea*, belongs to the FeS cluster containing group of the Rrf2 superfamily [91, 103]. NsrR functions as a regulator of the reactive nitrogen species (RNS) or nitric oxide (NO) induced stress response in many bacterial species. In most species, a common target of NsrR repression is the *hmp* gene, which encodes a flavohemoglobin enzyme that converts NO to nitrate (NO₃⁻) under aerobic conditions [91, 104].

The NsrR isolated from the obligate aerobe *S. coelicolor* is up to now the best characterized example, having been crystalized in both apo- and [4Fe-4S] forms (PDB 5N07, 5N08)(Fig. 4) [98, 105-109]. Although initially unclear, the relationship between [4Fe-4S] NsrR and an initially reported [2Fe-2S] form was found to be dependent upon 'protective' low molecular weight thiols added during purification [107, 110]. Through a combination of optical spectroscopies and time-resolved native MS it was demonstrated that [4Fe-4S] NsrR (17,824 Da) was quickly replaced by a [2Fe-2S] NsrR (17,647 Da) in the presence of DTT or β-mercaptoethanol under aerobic conditions. In contrast, [4Fe-4S] NsrR was entirely stable

under aerobic conditions, and bound tightly to DNA containing the *hmp1A* promoter, whereas apo- or [2Fe-2S] NsrR did not [107].

Upon exposure to NO, [4Fe-4S] NsrR undergoes a rapid and complex nitrosylation reaction that results in the loss of DNA binding [106, 107]. The reaction of NO with model FeS clusters results in a range of iron-nitrosyl species that have been well documented and include dinitrosyl iron complexes (DNICs, $\text{RFe}(\text{NO})_2$), Roussin's red ester (RRE, $\text{RFe}_2(\text{NO})_4$) and Roussin's black salt (RBS, $\text{Fe}_4\text{S}_3(\text{NO})_7$) [111, 112]. These studies have provide useful insight into protein-bound cluster nitrosylation reactions, which are harder to study. The end products of these protein cluster nitrosylations have been characterised using a range of techniques, including commonly applied absorbance and EPR spectroscopies, as well as the more specialised nuclear vibrational resonance spectroscopy (NRVS) [113, 114], revealing the formation of iron-nitrosyls similar in nature to the well characterised small molecule DNIC, RRE and RBS complexes [114, 115]. However, the precise nature of these iron-nitrosyls could not be unambiguously established by these methods because of the spectroscopic similarities of related iron-nitrosyl species.

LC-MS recently provided the first unambiguous identification of NsrR-bound RRE species. These were observed despite the denaturing conditions of LC-MS experiments, suggesting that RRE species exhibit particular chemical robustness [105]. We note that the coordination of NO at FeS clusters results in an accompanying redox process that may lead to the oxidation of cluster sulfide to sulfane (S^0) (e.g. see [114, 116]), resulting in this case in the observation of persulfide-coordinated RRE species. NO reactions carried out in the presence of glutathione or mycothiol gave rise to alternative oxidation reactions, resulting in protein S-thiolation at Cys 93 and Cys 99 of NsrR [105].

The identification of protein bound FeS cluster nitrosylation reaction intermediates has remained a major challenge due to the rapid rate of reaction and spectroscopic similarity of iron-nitrosyls when using optical and vibrational techniques [114, 117, 118]. Native MS offers the prospect of providing unprecedented levels of detail, but only if ways to probe such rapid reactions are available. While rapid-reaction kinetics MS is not yet feasible, alternative strategies have been employed that have begun to provide the level of detail required for full mechanistic elucidation.

In one approach, the NO releasing reagent dipropylenetriamine (DPTA) NONOate, which slowly liberates 2 moles of NO via a first order process, was chosen as the NO source [119, 120]. Under defined conditions, NO availability limited the reaction, enabling an *in situ* titration of [4Fe-4S] NsrR samples with NO during native MS experiments [109]. As noted above (section 3), the monomerization of dimeric NsrR during ionization was exploited to reduce sample complexity and assist data interpretation.

The peak at 17,824 Da due to monomeric [4Fe-4S] NsrR gradually decayed away, with the concomitant formation of a new peak 17,854 Da as the NO concentration increased. The newly formed +30 Da species, which initially increased in intensity before decaying away at [NO]:[4Fe-4S] ratios ≥ 3 , was consistent with the coordination of a single NO (+30 Da) molecule by the [4Fe-4S] cluster (Fig. 4b). A second species, +60 Da heavier and very likely corresponding to the coordination of two NO molecules, was also observed to increase in intensity, such that by [NO]:[4Fe-4S] ≈ 4 , it was at least as intense as the +30 Da adduct (Fig. 4b). Through the use of ^{34}S and ^{57}Fe isotopes, the +30 Da species was consistent with the formation of [4Fe-4S](NO); an unambiguous assignment of the +60 Da adduct as [4Fe-4S](NO)₂ could not be made due to overlapping species [109].

At [NO]:[4Fe-4S] ratios ≥ 4 a range of protein bound iron-nitrosyl species were detected. These occurred in the mass regions that corresponded to DNIC, RRE and RBS-like

species. The formation of DNICs (17,588 Da, $[\text{Fe}(\text{NO})_2]$) began almost immediately following the introduction of NO, but the vast majority of DNIC intensity was observed at $[\text{NO}]:[4\text{Fe-4S}]$ ratios ≥ 6 . A persulfide-coordinated RRE species (17,736 Da, $[\text{Fe}_2(\text{NO})_4(\text{S}^0)]$) also markedly increased in concentration at $[\text{NO}]:[4\text{Fe-4S}]$ ratios ≥ 6 (Fig. 4c) and reached a maximum by ~ 9 , consistent with earlier LC-MS observations. Multiple protein bound RBS-like species were also detected, with the general formula $[\text{Fe}_4(\text{S})_3(\text{NO})_x]$, where $x = 3$ to 6; RBS itself, $[\text{Fe}_4(\text{S})_3(\text{NO})_7]$, was not observed, though a species related to a putative $[\text{Fe}_4(\text{S})_2(\text{NO})_7]$ intermediate in the conversion of RRE to RBS was detected (Fig. 4d). We note that all RRE and RBS-like species exhibited a similar intensity profile, increasing markedly above $[\text{NO}]:[4\text{Fe-4S}] \geq 6$, suggesting the RRE to RBS interconversion, or breakdown of higher mass nitrosyl species [109].

The native MS data for NsrR, in combination with previous structural and biophysical data, provides the most complete picture thus far of the enigmatic process of FeS cluster nitrosylation (see Fig. 4e and [91, 109] for further details). Further investigations are required to establish the physiological significance of iron-nitrosyl intermediates and the effects of NO reaction on NsrR binding to DNA.

5. FeS clusters as sensors of O₂

Metabolic flexibility is a key feature of bacteria, enhancing survival during often rapid changes in their environment. Numerous bacteria can utilize O₂ as a terminal electron acceptor for respiration, with many capable of switching to a range of alternative electron acceptors when O₂ becomes limiting. In *E. coli* and many other bacteria the fumarate and nitrite reduction regulator (FNR) mediates a global response to O₂ deprivation and is the archetypal member of the FeS cluster-containing subfamily of the very diverse CRP superfamily [121].

Over several years, *E. coli* FNR was shown to utilise a $[4\text{Fe-4S}]$ cluster that undergoes a *simple* $[4\text{Fe-4S}]$ to $[2\text{Fe-2S}]$ cluster conversion in response to dissolved oxygen *in vitro* and *in vivo*, with concomitant loss of site-specific DNA binding. The integrity of the $[4\text{Fe-4S}]$ cluster is intricately linked to FNR function since it promotes dimerization, and hence site-specific DNA binding, and favourable contacts with the transcriptional machinery [122-131]. The discovery of a $[3\text{Fe-4S}]^{1+}$ cluster intermediate, and later a persulfide coordinated $[2\text{Fe-2S}]$ form, began to reveal a previously unrecognised complexity associated with the process of cluster conversion [126, 128, 132-134]. More recently, the structure of $[4\text{Fe-4S}]$ FNR from *Aliivibrio fischeri* has been reported (87% identity to *E. coli*; PDB 5E44, 5CVR), see Fig. 5a. Hence, the wealth of *in vitro* and *in vivo* data available for *E. coli* FNR can now be correlated with the structural insights gained from the *A. fischeri* homologue structure (see [28, 121, 135] for further details).

To try to gain further insight into the complexity of the FNR cluster conversion process, native MS was employed. The S24F variant of *E. coli* FNR is spectroscopically identical to wild type protein, following the same $[4\text{Fe-4S}]$ to $[2\text{Fe-2S}]$ conversion. However, it is kinetically distinct, as the initial reaction is ~ 4 fold slower [136], lending itself better to time-resolved native MS studies than the faster reacting wild type protein. Under anaerobic conditions the dimeric region of the spectrum was dominated by homo-dimeric $[4\text{Fe-4S}]$ FNR (59,796 Da) consistent with in solution studies.

Upon exposure to dissolved atmospheric O₂, three low intensity peaks due to dimers containing at least one $[3\text{Fe-4S}]$ cluster were observed, consistent with cluster conversion initiating the dimer to monomer transition [68, 136]. The monomeric region of the spectrum, dominated by $[4\text{Fe-4S}]$ FNR (29,898 Da), was exploited as above to reduce sample complexity and assist interpretation. Exposure to O₂ resulted in the formation of the previously reported

[3Fe-4S] and [2Fe-2S] forms, but also revealed a [3Fe-3S] form and single and double persulfide ligated forms of [2Fe-2S] FNR, along with persulfide adducts of apo-FNR [68] (Fig. 5b).

To investigate the kinetics of intermediate formation, [4Fe-4S] FNR was combined with excess dissolved O₂ and continuously infused into the ESI source of the instrument. Peaks corresponding to protein bound cluster intermediates (29,700 - 29,850 Da) reached a maximum ~15 to 30 min post O₂ exposure (Fig. 5c). In contrast, peaks corresponding to persulfide adducts of apo-FNR continued to gain intensity up to ~30 - 50 min post-exposure.

Global analysis, using Dynafit [100], was consistent with previous spectroscopic studies showing that the first step involves the ejection of Fe²⁺ from the [4Fe-4S] cluster. O₂ mediates oxidation of the cluster, leading to loss of an Fe²⁺, but does not result in formation of any oxygen adduct species. Whether O₂ reaction causes direct oxidation of [4Fe-4S]²⁺ to an unstable [4Fe-4S]³⁺ form that ejects Fe²⁺, or whether a RirA-like [4Fe-4S]²⁺ ⇌ [3Fe-4S]⁰ + Fe²⁺ equilibrium is in operation, with O₂ causing oxidation of [3Fe-4S]⁰ to [3Fe-4S]¹⁺ as the committed step to conversion is currently unclear. Once formed the [3Fe-4S]¹⁺ cluster is only transiently stable, ejecting S²⁻ to generate the [3Fe-3S] intermediate [68]. Independent evidence for the existence of a protein bound [3Fe-3S]³⁺ cluster derives from ESI Fourier transform ion cyclotron resonance MS studies on the [3Fe-4S] cluster of *Pyrococcus furiosus* FdI [137]. The decay of the [3Fe-3S] intermediate was found to be relatively slow and represents the rate-limiting step in the [3Fe-4S] to [2Fe-2S] conversion process; the observed rate constant (from native MS data) being comparable to that previously reported for the [3Fe-4S] to [2Fe-2S] conversion of the wild type and S24F FNR proteins in solution [68, 136]. We note that if [3Fe-3S] cluster intermediate adopts a planer arrangement, as observed for a recently reported small molecule complex, it would suggest a means by which the cuboidal [4Fe-4S] cluster and associated tetrahedral array of ligands, might rearrange to give a [2Fe-2S] rhomb with a planer arrangement of the same coordinating ligands (Cys 20, 23, 29 and 122) as for the [4Fe-4S] cluster [68].

Resonance Raman studies previously showed that FNR cluster sulfide can become oxidized to sulfane during the cluster conversion leading to persulfide ligated [2Fe-2S] cluster [134]. Both the [2Fe-3S] and [2Fe-4S] species (single and double persulfide-coordinated [2Fe-2S] cluster, respectively) maximised well before the [2Fe-2S] cluster (~30 min), see Fig. 5c. Global analysis of the data showed that [2Fe-3S] is not formed from the [2Fe-2S] cluster or vice versa; rather, the [3Fe-3S] cluster decomposes to give rise to both the [2Fe-3S] and [2Fe-2S] clusters. Similarly, the [2Fe-4S] forms from the [3Fe-4S] cluster and not the [3Fe-3S] cluster. These processes represent an oxidative branching of the main cluster conversion pathway, rather than occurring post-cluster conversion due to S⁰ incorporation (Fig. 5d). The kinetics of persulfide formation on apo-FNR were also followed by LC-MS, but the details are beyond the scope of this review; see [68] for further details. As noted above, ³⁴S/⁵⁷Fe isotope substitution data were crucial for the unambiguous confirmation of the species, and thus, mechanism discussed here [68, 99, 101, 102].

6. Future perspectives/Conclusion

Native MS is a powerful methodology that can yield detailed information on multiple species simultaneously, in favourable cases in real time, opening up the possibility of global kinetic studies as well a rapid reaction kinetics [138, 139]. Thus, the technique has enormous potential to provide an unprecedented level of insight into protein mechanism and, thus, function. Thanks to improvements in modern MS hardware, even entry level ESI-TOF

instruments have the potential to be applied in this way, making the methodology highly accessible. Optimisation of ionization and other instrument parameters is normally required [61], however, meaning that the technique is not yet multi-user walk up. Some newer *hybrid* instruments now incorporate ion mobility methodologies for the enhanced separation of closely related species, providing access to molecular architecture in addition to mass [41], and adding further to the ways in which native MS can be applied, with even greater sensitivity.

The work highlighted here illustrates multiple examples of how native MS has been recently applied to the study of protein bound FeS cluster cofactors, and to protein-protein interactions that are integral to FeS cluster biosynthesis. Continuing advances in hardware, including the incorporation of ion mobility separation, makes accessible ever larger cofactor-protein complexes. The scene is now set for much broader application of native MS to studies of a wide range of protein-cofactor systems.

Declaration of Competing Interest

The authors declare that they have no known competing financial interests or personal relationships that could have appeared to influence the work reported in this paper.

Acknowledgments

This work was supported by Biotechnology and Biological Sciences Research Council (BBSRC) of the UK through grants BB/P006140/1 and BB/S001018/1.

References

- [1] W. Maret, *Adv Exp Med Biol*, 1055 (2018) 1-20.
- [2] P.L. Hagedoorn, *Proteomes*, 3 (2015) 424-439.
- [3] J.B. Howard, D.C. Rees, *Adv Protein Chem*, 42 (1991) 199-280.
- [4] C.J. Reedy, B.R. Gibney, *Chem Rev*, 104 (2004) 617-649.
- [5] P. Zanello, *J Struct Biol*, 200 (2017) 1-19.
- [6] P. Zanello, *J Struct Biol*, 202 (2018) 250-263.
- [7] P. Zanello, *J Struct Biol*, 202 (2018) 264-274.
- [8] P. Zanello, *J Struct Biol*, 205 (2019) 103-120.
- [9] M.K. Johnson, *Curr Opin Chem Biol*, 2 (1998) 173-181.
- [10] H. Beinert, R.H. Holm, E. Munck, *Science*, 277 (1997) 653-659.
- [11] S. Bailey, *Nat Chem Biol*, 8 (2011) 24-25.
- [12] S. Bian, J.A. Cowan, *Coord Chem Revs*, 190-192 (1999) 1049-1066.
- [13] W.E. Broderick, J.B. Broderick, *J Biol Inorg Chem*, 24 (2019) 769-776.
- [14] M.T. Werth, H. Sices, G. Cecchini, I. Schroder, S. Lasage, R.P. Gunsalus, M.K. Johnson, *FEBS Lett*, 299 (1992) 1-4.
- [15] A. Volbeda, M.T. Pellicer Martinez, J.C. Crack, P. Amara, O. Gigarel, J.T. Munnoch, M.I. Hutchings, C. Darnault, N.E. Le Brun, J.C. Fontecilla-Camps, *J Am Chem Soc*, 141 (2019) 2367-2375.
- [16] A.S. Fleischhacker, A. Stubna, K.L. Hsueh, Y. Guo, S.J. Teter, J.C. Rose, T.C. Brunold, J.L. Markley, E. Munck, P.J. Kiley, *Biochemistry*, 51 (2012) 4453-4462.
- [17] J.A. Hernandez, L. Curatti, C.P. Aznar, Z. Perova, R. D. Britt, L.M. Rubio, *Proc Natl Acad Sci U S A* 105 (2008):11679-11684.
- [18] Y. Shomura, K.S. Yoon, H. Nishihara, Y. Higuchi, *Nature*, 479 (2011) 253-256.
- [19] L. Noodleman, C.Y. Peng, D.A. Case, J.M. Mouesca, *Coord Chem Rev*, 144 (1995) 199-244.
- [20] J.M. Mouesca, L. Noodleman, D.A. Case, B. Lamotte, *Inorg Chem*, 34 (1995) 4347-4359.
- [21] J.A. Imlay, *Mol Microbiol*, 59 (2006) 1073-1082.

- [22] Y. Guo, J. Li, in T. A. Rouault (Ed), Iron-sulfur clusters in chemistry and biology: Characterization, properties and application, 2nd ed., De Gruyter, Berlin, 2017, pp 77-134.
- [23] W.R. Hagen, *J Biol Inorg Chem*, 23 (2018) 623-634.
- [24] D.T. Petasis, M.P. Hendrichs, in T. A. Rouault (Ed), Iron-sulfur clusters in chemistry and biology: Characterization, properties and application, 2nd ed., De Gruyter, Berlin, 2017, pp 135-162.
- [25] M. Chakrabarti, P.A. Lindahl, in T. A. Rouault (Ed), Iron-sulfur clusters in chemistry and biology: Characterization, properties and application, 2nd ed., De Gruyter, Berlin, 2017, pp 163-190
- [26] M.E. Pandelia, N.D. Lanz, S.J. Booker, C. Krebs, *Biochim Biophys Acta*, 1853 (2015) 1395-1405.
- [27] S. Todorovic, M. Teixeira, *J Biol Inorg Chem*, 23 (2018) 647-661.
- [28] A. Volbeda, C. Darnault, O. Renoux, Y. Nicolet, J.C. Fontecilla-Camps, *Sci Adv*, 1 (2015) e1501086.
- [29] K. Cai, J.L. Markley, *Molecules*, 23 (2018) 2213.
- [30] S.J. Maiocco, L.M. Walker, S.J. Elliott, *Methods Enzymol*, 606 (2018) 319-339.
- [31] A.J. Thomson, J. Breton, S.J. George, J.N. Butt, F.A. Armstrong, E.C. Hatchikian, *Biochem Soc Trans*, 19 (1991) 594-599.
- [32] L. Noodleman, in T. A. Rouault (Ed), Iron-sulfur clusters in chemistry and biology: Characterization, properties and application, 2nd ed., De Gruyter, Berlin, 2017, pp 21-76
- [33] L. Noodleman, T. Lovell, T. Liu, F. Himu, R.A. Torres, *Curr Opin Chem Biol*, 6 (2002) 259-273.
- [34] J.C. Crack, P. Amara, A. Volbeda, J.M. Mousesca, R. Rohac, M.T. Pellicer Martinez, C.Y. Huang, O. Gigarel, C. Rinaldi, N.E. Le Brun, J.C. Fontecilla-Camps, *J Am Chem Soc*, 142 (2020) 5104-5116.
- [35] V. Katta, B.T. Chait, *J Am Chem Soc*, 113 (1991) 8534-8535.
- [36] J.M. Moulis, N. Scherrer, J. Gagnon, E. Forest, Y. Petillot, D. Garcia, *Arch Biochem Biophys*, 305 (1993) 186-192.
- [37] P.F. Hu, J.A. Loo, *J Mass Spectrom*, 30 (1995) 1076-1082.
- [38] J. Zaia, D. Fabris, D. Wei, R.L. Karpel, C. Fenselau, *Protein Sci*, 7 (1998) 2398-2404.
- [39] D.R. Gumerov, I.A. Kaltashov, *Anal Chem*, 73 (2001) 2565-2570.
- [40] J.A. Loo, *Mass Spectrom Rev*, 16 (1997) 1-23.
- [41] S.A. Chandler, J.L. Benesch, *Curr Opin Chem Biol*, 42 (2018) 130-137.
- [42] A.C. Leney, A.J. Heck, *J Am Soc Mass Spectrom*, 28 (2017) 5-13.
- [43] A.J. Heck, *Nat Methods*, 5 (2008) 927-933.
- [44] O.I. Leszczyszyn, C.A. Blindauer, *Phys Chem Chem Phys*, 12 (2010) 13408-13418.
- [45] S. Perez-Rafael, S. Atrian, M. Capdevila, O. Palacios, *Talanta*, 83 (2011) 1057-1061.
- [46] J. Ross, T. Lambert, C. Piergentili, D. He, K.J. Waldron, C.L. Mackay, J. Marles-Wright, D.J. Clarke, *Chem Commun*, 56 (2020) 3417-3420.
- [47] J.S. Scheller, G.W. Irvine, M.J. Stillman, *Dalton Trans*, 47 (2018) 3613-3637.
- [48] D.B. Ott, A. Hartwig, M.J. Stillman, *Metallomics*, 11 (2019) 968-981.
- [49] F. Lermyte, J. Everett, Y.P.Y. Lam, C.A. Wootton, J. Brooks, M.P. Barrow, N.D. Telling, P.J. Sadler, P.B. O'Connor, J.F. Collingwood, *J Am Soc Mass Spectrom*, 30 (2019) 2123-2134.
- [50] M.A. Maniero, R.G. Wuilloud, E.A. Callegari, P.N. Smichowski, M.A. Fanelli, *J Trace Elem Med Biol*, 58 (2020) 126441.
- [51] D.J. Hare, A. Rembach, B.R. Roberts, *Meth Mol Biol*, 1303 (2016) 379-389.
- [52] R. Puglisi, E. Boeri Erba, A. Pastore, *FEBS J*, 287 (2020) 2428-2439.
- [53] C.W. Lin, J.W. McCabe, D.H. Russell, D.P. Barondeau, *J Am Chem Soc*, 142 (2020) 6018-6029.
- [54] M. Jia, S. Sen, C. Wachnowsky, I. Fidai, J.A. Cowan, V.H. Wysocki, *Angew Chem Int Ed*, 59 (2020) 6724-6728.

- [55] S. Gervason, D. Larkem, A.B. Mansour, T. Botzanowski, C.S. Muller, L. Pecqueur, G. Le Pavec, A. Delaunay-Moisan, O. Brun, J. Agramunt, A. Grandas, M. Fontecave, V. Schunemann, S. Cianferani, C. Sizun, M.B. Toledano, B. D'Autreaux, *Nat Commun*, 10 (2019) 3566.
- [56] D.W. Woodall, C.J. Brown, S.A. Raab, T.J. El-Baba, A. Laganowsky, D.H. Russell, D.E. Clemmer, *Anal Chem*, 92 (2020) 3440-3446.
- [57] K.L. Kay, C.J. Hamilton, N.E. Le Brun, *J Inorg Biochem*, 190 (2019) 24-30.
- [58] L. Zhou, K.L. Kay, O. Hecht, G.R. Moore, N.E. Le Brun, *Biochim Biophys Acta Proteins Proteom*, 1866 (2018) 275-282.
- [59] S.P. Bennett, M.J. Soriano-Laguna, J.M. Bradley, D.A. Svistunenko, D.J. Richardson, A.J. Gates, N.E. Le Brun, *Chem Sci*, 10 (2019) 4985-4993.
- [60] C.A. Blindauer, N.C. Polfer, S.E. Keiper, M.D. Harrison, N.J. Robinson, P.R. Langridge-Smith, P.J. Sadler, *J Am Chem Soc*, 125 (2003) 3226-3227.
- [61] J.C. Crack, N.E. Le Brun, in: J.M. Walker (Ed.) *Meth Mol Biol*, Nature-Springer, 2021. ISBN 978-1-0716-1604-8
- [62] F.D. Kondrat, G.R. Kowald, C.A. Scarff, J.H. Scrivens, C.A. Blindauer, *Chem Commun*, 49 (2013) 813-815.
- [63] I.A. Kaltashov, J.W. Pawlowski, W. Yang, K. Muneeruddin, H. Yao, C.E. Bobst, A.N. Lipatnikov, *Methods*, 144 (2018) 14-26.
- [64] C. Bich, S. Baer, M.C. Jecklin, R. Zenobi, *J Am Soc Mass Spectrom*, 21 (2010) 286-289.
- [65] A.J.R. Heck, R.H.H. van den Heuvel, *Mass Spectrom Rev*, 23 (2004) 368-389.
- [66] F. Sobott, M.G. McCammon, H. Hernandez, C.V. Robinson, *Phil Trans A, Math Phys Eng Sci*, 363 (2005) 379-389.
- [67] K.A. Johnson, M.F. Verhagen, P.S. Brereton, M.W. Adams, I.J. Amster, *Anal Chem*, 72 (2000) 1410-1418.
- [68] J.C. Crack, A.J. Thomson, N.E. Le Brun, *Proc Natl Acad Sci U S A*, 114 (2017) E3215-E3223.
- [69] K.S. Hagen, J.G. Reynolds, R.H. Holm, *J Am Chem Soc*, 103 (1981) 4054-4063.
- [70] S.A. Freibert, B.D. Weiler, E. Bill, A.J. Pierik, U. Muhlenhoff, R. Lill, *Meth Enzymol*, 599 (2018) 197-226.
- [71] J.J. Braymer, S.A. Freibert, M. Rakwalska-Bange, R. Lill, *Biochim Biophys Acta Mol Cell Res*, 1868 (2021) 118863.
- [72] B. Blanc, C. Gerez, S. Ollagnier de Choudens, *Biochim Biophys Acta*, 1853 (2015) 1436-1447.
- [73] A.D. Tsaousis, *Front Microbiol*, 10 (2019) 2478.
- [74] E.L. Mettert, P.J. Kiley, *Annu Rev Microbiol*, 69 (2015) 505-526.
- [75] R. Shi, A. Proteau, M. Villarroya, I. Moukadiri, L. Zhang, J.F. Trempe, A. Matte, M.E. Armengod, M. Cygler, *PLoS Biol*, 8 (2010) e1000354.
- [76] J.H. Kim, M. Tonelli, T. Kim, J.L. Markley, *Biochemistry*, 51 (2012) 5557-5563.
- [77] Y. Shimomura, K. Wada, K. Fukuyama, Y. Takahashi, *J Mol Biol*, 383 (2008) 133-143.
- [78] E.N. Marinoni, J.S. de Oliveira, Y. Nicolet, E.C. Raulfs, P. Amara, D.R. Dean, J.C. Fontecilla-Camps, *Angew Chem Int Ed*, 51 (2012) 5439-5442.
- [79] S. Sato, Y. Matsushima, M. Kanazawa, N. Tanaka, T. Fujishiro, K. Kunichika, R. Nakamura, H. Tomioka, K. Wada, Y. Takahashi, *Mol Microbiol*, (2020).
- [80] J.H. Kim, A.K. Fuzery, M. Tonelli, D.T. Ta, W.M. Westler, L.E. Vickery, J.L. Markley, *Biochemistry*, 48 (2009) 6062-6071.
- [81] J.L. Markley, J.H. Kim, Z. Dai, J.R. Bothe, K. Cai, R.O. Frederick, M. Tonelli, *FEBS Lett*, 587 (2013) 1172-1179.
- [82] M. Nuth, T. Yoon, J.A. Cowan, *J Am Chem Soc*, 124 (2002) 8774-8775.
- [83] B.E. Lewis, Z. Mason, A.V. Rodrigues, M. Nuth, E. Dizin, J.A. Cowan, T.L. Stemmler, *Metallomics*, 11 (2019) 1820-1835.
- [84] A.V. Rodrigues, A. Kandegedara, J.A. Rotondo, A. Dancis, T.L. Stemmler, *Biometals*, 28 (2015) 567-576.
- [85] K. Keyser, J.A. Imlay, *Proc Natl Acad Sci U S A*, 93 (1996) 13635-13640.

- [86] T.A. Ramelot, J.R. Cort, S. Goldsmith-Fischman, G.J. Kornhaber, R. Xiao, R. Shastry, T.B. Acton, B. Honig, G.T. Montelione, M.A. Kennedy, *J Mol Biol*, 344 (2004) 567-583.
- [87] J. Li, X. Ren, B. Fan, Z. Huang, W. Wang, H. Zhou, Z. Lou, H. Ding, J. Lyu, G. Tan, *Appl Environ Microbiol*, 85 (2019) e01967-18.
- [88] C.E. Outten, T.V. O'Halloran, *Science*, 292 (2001) 2488-2492.
- [89] S. Adinolfi, R. Puglisi, J.C. Crack, C. Iannuzzi, F. Dal Piaz, P.V. Konarev, D.I. Svergun, S. Martin, N.E. Le Brun, A. Pastore, *Front Mol Biosci*, 4 (2017) 97.
- [90] S. Rajagopalan, S.J. Teter, P.H. Zwart, R.G. Brennan, K.J. Phillips, P.J. Kiley, *Nat Struct Mol Biol*, 20 (2013) 740-747.
- [91] J.C. Crack, A. Volbeda, N.E. Le Brun, J.C. Fontecilla-Camps, in: *Encyclopedia of Inorganic and Bioinorganic Chemistry*, Wiley, 2020, pp. 1-23.
- [92] A.W. Johnston, J.D. Todd, A.R. Curson, S. Lei, N. Nikolaidou-Katsaridou, M.S. Gelfand, D.A. Rodionov, *Biometals*, 20 (2007) 501-511.
- [93] M.T. Pellicer Martinez, A.B. Martinez, J.C. Crack, J.D. Holmes, D.A. Svistunenko, A.W.B. Johnston, M.R. Cheesman, J.D. Todd, N.E. Le Brun, *Chem Sci*, 8 (2017) 8451-8463.
- [94] J.D. Todd, G. Sawers, A.W.B. Johnston, *Molecular Genetics and Genomics*, 273 (2005) 197-206.
- [95] J.D. Todd, M. Wexler, G. Sawers, K.H. Yeoman, P.S. Poole, A.W. Johnston, *Microbiology*, 148 (2002) 4059-4071.
- [96] C. Singleton, G.F. White, J.D. Todd, S.J. Marritt, M.R. Cheesman, A.W. Johnston, N.E. Le Brun, *J Biol Chem*, 285 (2010) 16023-16031.
- [97] M. Behringer, L. Plotzky, D. Baabe, M.K. Zaretzke, P. Schweyen, M. Broring, D. Jahn, E. Hartig, *Biochem J*, 477 (2020) 191-212.
- [98] A. Volbeda, E.L. Dodd, C. Darnault, J.C. Crack, O. Renoux, M.I. Hutchings, N.E. Le Brun, J.C. Fontecilla-Camps, *Nat Commun*, 8 (2017) 15052.
- [99] M.T. Pellicer Martinez, J.C. Crack, M.Y. Stewart, J.M. Bradley, D.A. Svistunenko, A.W. Johnston, M.R. Cheesman, J.D. Todd, N.E. Le Brun, *Elife*, 8 (2019).
- [100] P. Kuzmic, *Meth Enzymol*, 467 (2009) 247-280.
- [101] J.C. Crack M.Y.Y. Stewart, N.E. Le Brun, *Biol Meth Prot*, 4 (2019) byp015.
- [102] J.C. Crack, J. Green, A.J. Thomson, N.E. Le Brun, *Meth Mol Biol*, 1122 (2014) 33-48.
- [103] H.J. Beaumont, S.I. Lens, W.N. Reijnders, H.V. Westerhoff, R.J. van Spanning, *Mol Microbiol*, 54 (2004) 148-158.
- [104] J.D. Partridge, D.M. Bodenmiller, M.S. Humphrys, S. Spiro, *Mol Microbiol*, 73 (2009) 680-694.
- [105] J.C. Crack, C.J. Hamilton, N.E. Le Brun, *Chem Commun*, 54 (2018) 5992-5995.
- [106] J.C. Crack, D.A. Svistunenko, J. Munnoch, A.J. Thomson, M.I. Hutchings, N.E. Le Brun, *J Biol Chem*, 291 (2016) 8663-8672.
- [107] J.C. Crack, J. Munnoch, E.L. Dodd, F. Knowles, M.M. Al Bassam, S. Kamali, A.A. Holland, S.P. Cramer, C.J. Hamilton, M.K. Johnson, A.J. Thomson, M.I. Hutchings, N.E. Le Brun, *J Biol Chem*, 290 (2015) 12689-12704.
- [108] N.P. Tucker, M.G. Hicks, T.A. Clarke, J.C. Crack, G. Chandra, N.E. Le Brun, R. Dixon, M.I. Hutchings, *PLoS One*, 3 (2008) e3623.
- [109] J.C. Crack, N. Le Brun, *Chemistry*, 25 (2019) 3675-3684.
- [110] N.P. Tucker, N.E. Le Brun, R. Dixon, M.I. Hutchings, *Trends Microbiol*, 18 (2010) 149-156.
- [111] A.R. Butler, Glidewell, C., and Li, M., *Adv Inorg Chem*, 32 (1988) 335-393.
- [112] A.R. Butler, I.L. Megson, *Chem Rev*, 102 (2002) 1155-1166.
- [113] J.C. Crack, J. Green, A.J. Thomson, N.E. Le Brun, *Acc Chem Res*, 47 (2014) 3196-3205.
- [114] P.N. Serrano, H. Wang, J.C. Crack, C. Prior, M.I. Hutchings, A.J. Thomson, S. Kamali, Y. Yoda, J. Zhao, M.Y. Hu, E.E. Alp, V.S. Oganessian, N.E. Le Brun, S.P. Cramer, *Angew Chem Int Ed*, 55 (2016) 14575-14579.
- [115] H. Lewandowska, M. Kalinowska, K. Brzoska, K. Wojciuk, G. Wojciuk, M. Kruszewski, *Dalton Trans*, 40 (2011) 8273-8289.

- [116] J.C. Crack, L.J. Smith, M.R. Stapleton, J. Peck, N.J. Watmough, M.J. Buttner, R.S. Buxton, J. Green, V.S. Oganessian, A.J. Thomson, N.E. Le Brun, *J Am Chem Soc*, 133 (2011) 1112-1121.
- [117] Z.J. Tonzetich, H. Wang, D. Mitra, C.E. Tinberg, L.H. Do, F.E. Jenney, Jr., M.W. Adams, S.P. Cramer, S.J. Lippard, *J Am Chem Soc*, 132 (2010) 6914-6916.
- [118] D.B. Grabarczyk, P.A. Ash, W.K. Myers, E.L. Dodd, K.A. Vincent, *Dalton Trans*, 48 (2019) 13960-13970.
- [119] L.K. Keefer, R.W. Nims, K.M. Davies, D.A. Wink, *Meth Enzymol*, 268 (1996) 281-293.
- [120] E. Rivera-Tirado, M. Lopez-Casillas, C. Wesdemiotis, *Rapid Commun Mass Spectrom*, 25 (2011) 3581-3586.
- [121] A. Volbeda, Y. Nicolet, J.C. Fontecilla-Camps, Fumarate and Nitrate Reduction Regulator (FNR), in: *Encyclopedia of Inorganic and Bioinorganic Chemistry*, pp. 1-11.
- [122] B.A. Lazizzera, D.M. Bates, P.J. Kiley, *Genes Dev*, 7 (1993) 1993-2005.
- [123] B.A. Lazizzera, H. Beinert, N. Khoroshilova, M.C. Kennedy, P.J. Kiley, *J Biol Chem*, 271 (1996) 2762-2768.
- [124] N. Khoroshilova, H. Beinert, P.J. Kiley, *Proc Natl Acad Sci U S A*, 92 (1995) 2499-2503.
- [125] J. Green, B. Bennett, P. Jordan, E.T. Ralph, A.J. Thomson, J.R. Guest, *Biochem J*, 316 (1996) 887-892.
- [126] J. Crack, J. Green, A.J. Thomson, *J Biol Chem*, 279 (2004) 9278-9286.
- [127] N. Khoroshilova, C. Popescu, E. Munck, H. Beinert, P.J. Kiley, *Proc Natl Acad Sci U S A*, 94 (1997) 6087-6092.
- [128] J.C. Crack, A.A. Gaskell, J. Green, M.R. Cheesman, N.E. Le Brun, A.J. Thomson, *J Am Chem Soc*, 130 (2008) 1749-1758.
- [129] V.R. Sutton, E.L. Mettert, H. Beinert, P.J. Kiley, *J Bacteriol*, 186 (2004) 8018-8025.
- [130] K.E. Lamberg, C. Luther, K.D. Weber, P.J. Kiley, *J Mol Biol*, 315 (2002) 275-283.
- [131] C.V. Popescu, D.M. Bates, H. Beinert, E. Munck, P.J. Kiley, *Proc Natl Acad Sci U S A*, 95 (1998) 13431-13435.
- [132] J.C. Crack, J. Green, M.R. Cheesman, N.E. Le Brun, A.J. Thomson, *Proc Natl Acad Sci U S A*, 104 (2007) 2092-2097.
- [133] J.C. Crack, J. Green, N.E. Le Brun, A.J. Thomson, *J Biol Chem*, 281 (2006) 18909-18913.
- [134] B. Zhang, J.C. Crack, S. Subramanian, J. Green, A.J. Thomson, N.E. Le Brun, M.K. Johnson, *Proc Natl Acad Sci U S A*, 109 (2012) 15734-15739.
- [135] E.L. Mettert, P.J. Kiley, *Antioxid Redox Signal*, 29 (2018) 1830-1840.
- [136] A.J. Jervis, J.C. Crack, G. White, P.J. Artymiuk, M.R. Cheesman, A.J. Thomson, N.E. Le Brun, *J. Green, P Natl Acad Sci USA*, 106 (2009) 4659-4664.
- [137] K.A. Johnson, I.J. Amster, *J Am Soc Mass Spectrom*, 12 (2001) 819-825.
- [138] P.V. Attwood, M.A. Geeves, *Anal Biochem*, 334 (2004) 382-389.
- [139] G.W. Irvine, K.E. Duncan, M. Gullons, M.J. Stillman, *Chemistry*, 21 (2015) 1269-1279.
- [140] J. Fritsch, P. Scheerer, S. Frielingsdorf, S. Kroschinsky, B. Friedrich, O. Lenz, C.M. Spahn, *Nature*, 479 (2011) 249-252.
- [141] Y. Lee, R. Jeon le, K.A. Abboud, R. Garcia-Serres, J. Shearer, L.J. Murray, *Chem Commun*, 52 (2016) 1174-1177.
- [142] E.F. Pettersen, T.D. Goddard, C.C. Huang, G.S. Couch, D.M. Greenblatt, E.C. Meng, T.E. Ferrin, *J Comp Chem*, 25 (2004) 1605-1612.

Figure legends

Figure 1. Examples of protein-associated iron-sulfur clusters. [2Fe-2S] cluster from *Streptomyces venezuelae* RsrR, with unusual cluster coordination involving three different types of amino acid residues (PDB 6HSE) [15]. [3Fe-4S], [4Fe-3S] and [4Fe-4S] clusters are from an O₂-tolerant [NiFe]-hydrogenase from the aerobic H₂ oxidizer *Ralstonia eutropha* H16 (PDB 3RGW) [140]. The [4Fe-3S] cluster, which is coordinated by six cysteines, is thus far unique. The planer hexagonal arrangement of the proposed [3Fe-3S] cluster conversion intermediate is based on the inorganic model [Fe₃S₃]³⁺ reported by Lee *et al.* [141]. Protein/cofactor structural graphics here, and elsewhere, were generated using UCSF Chimera [142].

Figure 2. IscS-IscU interactions and FeS cluster assembly. (a) Ribbon diagram representing the structure of *Archaeoglobus fulgidus* (IscS)₂(IscU)₂, with PLP and [2Fe-2S] cluster cofactors indicated in space filling mode (PDB 4EB5) [78]. (b) Native mass spectrometry data showing the presence of *Escherichia coli* (IscS)₂, (IscS)₂(IscU) and (IscS)₂(IscU)₂ [89]. (c) Schematic mechanism of IscSU-mediated FeS biogenesis, based on native MS data, with iron binding as the first step [53].

Figure 3. The iron and O₂-sensor RirA. (a) Ribbon diagram model of the structure of *Rhizobium leguminosarum* RirA, generated using Swissmodel, based on the structure of NsrR (PDB 5N07) [98, 99]. The DNA recognition helix is indicated by an asterisk. (b) Native MS data for *R. leguminosarum* RirA, showing the presence of a [4Fe-4S] cluster in the as prepared protein (black line) along with various cluster breakdown species [99]. Exposure to and iron chelator (simulating low iron conditions) resulted in the loss of the cluster. The spectrum in grey was recorded after 4 mins, and that in red after 30 mins. Abundant and mechanistically important species are labelled. (c) Time-resolved MS data monitoring the loss of cluster from RirA under low iron conditions. Various species are plotted, as indicated, in the two panels. Solid lines represent fits generated using a mechanistic model of the reaction, which is depicted in (d). The iron-sensing step is proposed to be the initial dissociation/re-association of a Fe²⁺ from/to a [3Fe-4S]⁰ species. The O₂-sensing step is proposed to be the oxidation of the resulting [3Fe-4S]⁰ cluster to [3Fe-4S]¹⁺ [99].

Figure 4. The nitric oxide (NO) sensor NsrR. (a) Ribbon diagram of the structure of the *Streptomyces coelicolor* NsrR homodimer, with the cluster shown in space-filling mode (PDB 5N07) [98]. The DNA recognition helix is indicated by an asterisk. (b) Native MS data for *S. coelicolor* NsrR in the absence and presence of increasing amounts of NO. Major species are labelled [109]. The species at +58 Da (relative to [4Fe-4S] NsrR) in the as prepared spectrum is due to an unknown contaminant. (c) and (d) Native MS data before and after the addition of 11 NO per cluster, showing mass regions containing DNIC- and RRE-type species (c) and RBS-type species (d), as indicated. (e) Mechanistic scheme, based on native MS and other data, for the nitrosylation of the NsrR [4Fe-4S] cluster. Loss of DNA binding refers to the *hmpA2* promoter region.

Figure 5. The O₂ sensor FNR. (a) Ribbon diagram of the structure of FNR from *Aliivibrio fischeri* (PDB 5E44) [28]. The [4Fe-4S] cluster is shown in space-filling mode, and the DNA recognition helix is indicated by an asterisk. (b) Native MS data for the as prepared protein before (black line) and after (red line) exposure to O₂ for 18 min [68]. Major species are as

indicated. (c) Time-resolved MS data monitoring FNR cluster conversion upon exposure to O₂ as a function of time. Various species are plotted, as indicated, in the two panels. Solid lines represent fits generated using a mechanistic model of the reaction (see [68] for further details), which is depicted in (d). Conversion of the [4Fe-4S] cluster results in dissociation of dimeric FNR into monomers. Native MS data indicates that this occurs as the [3Fe-4S] species is formed, as indicated [68].

Figures

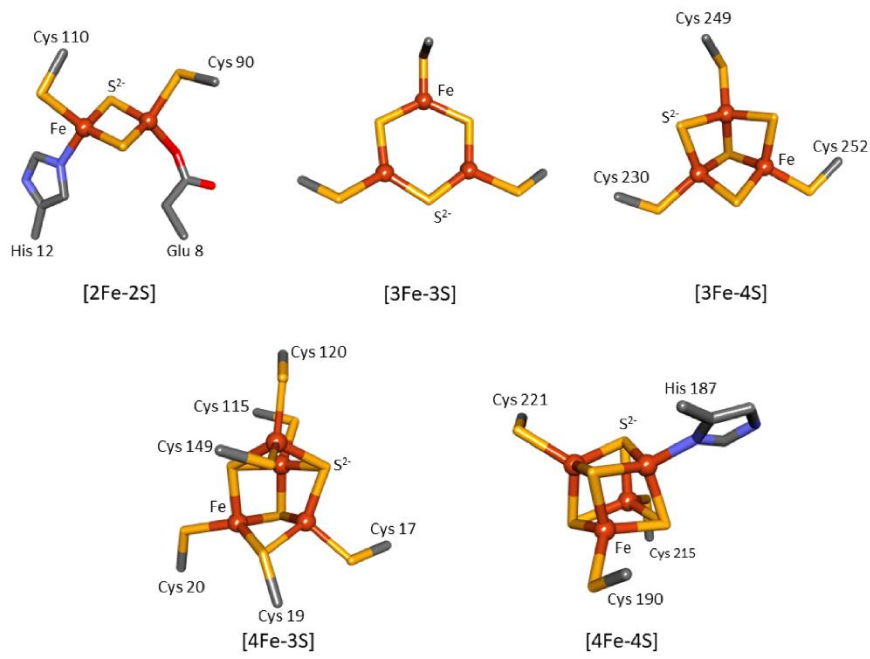


Figure 1

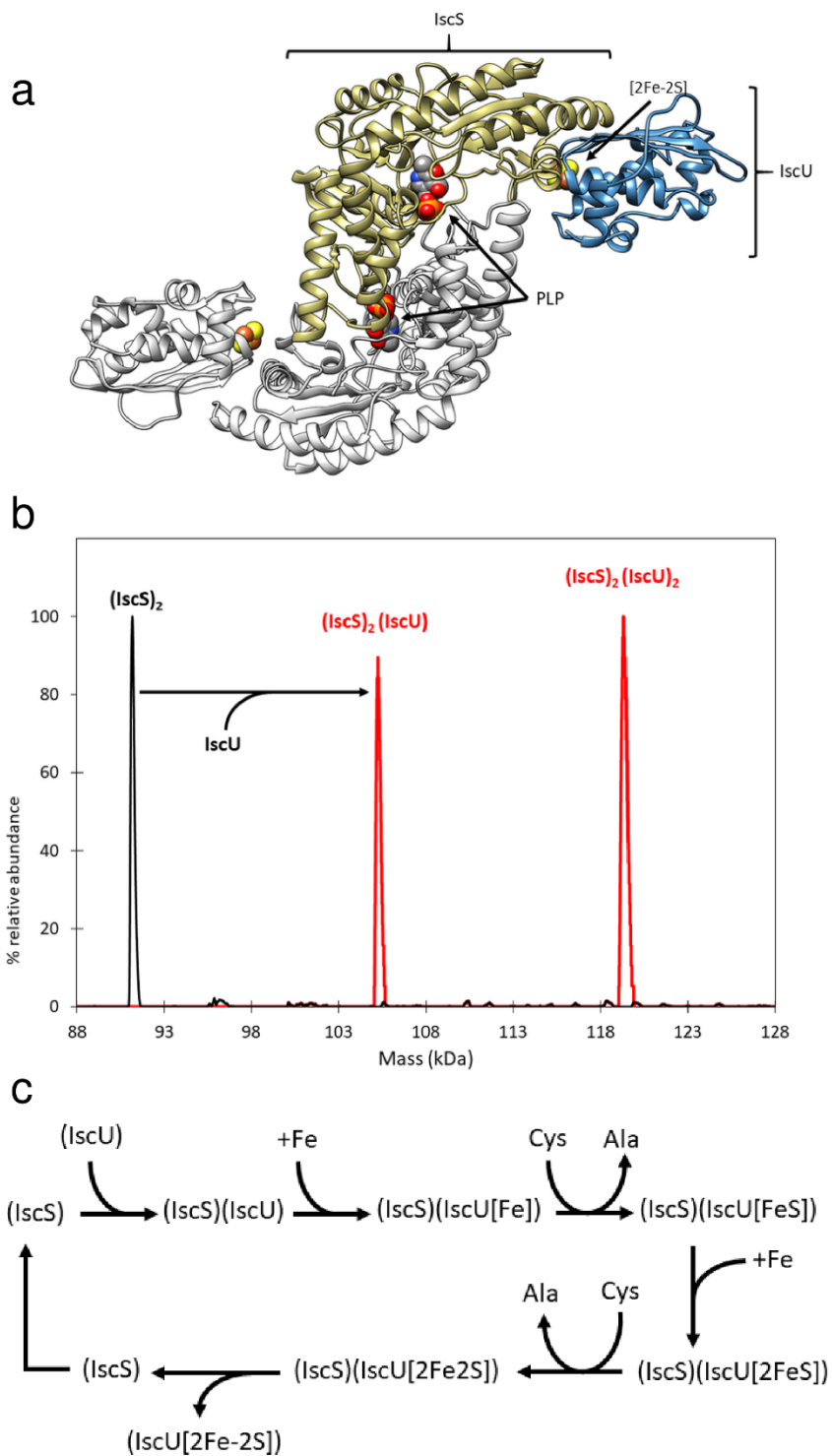


Figure 2

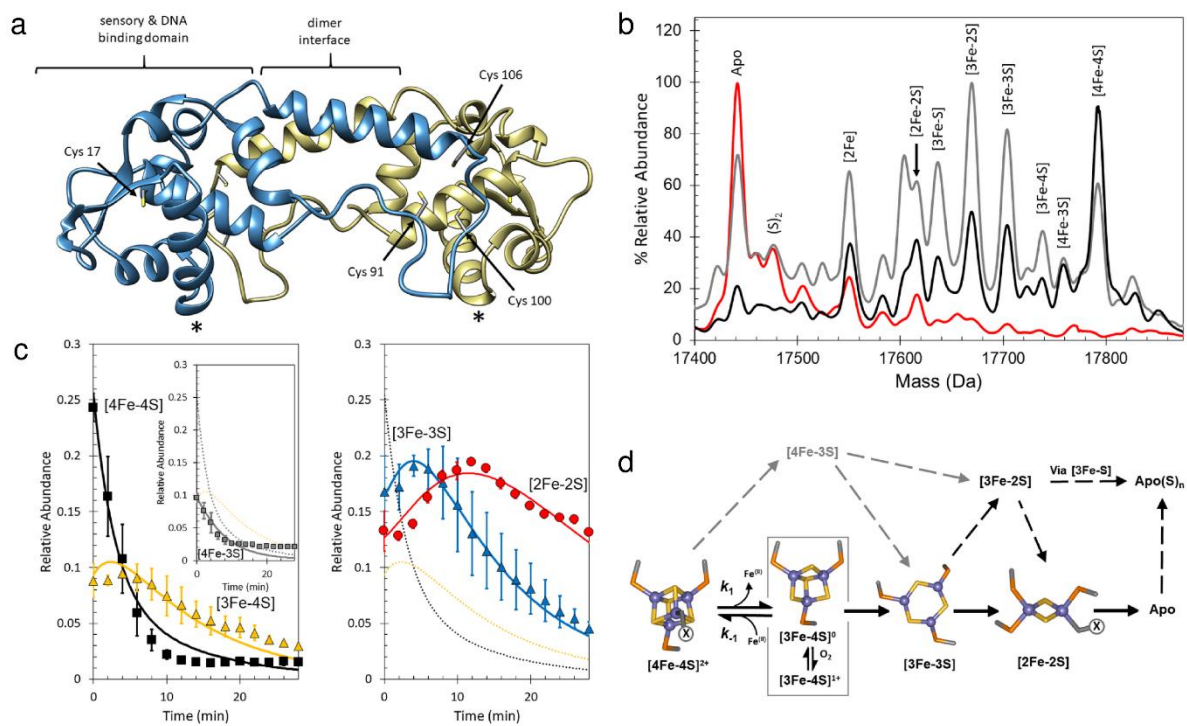


Figure 3

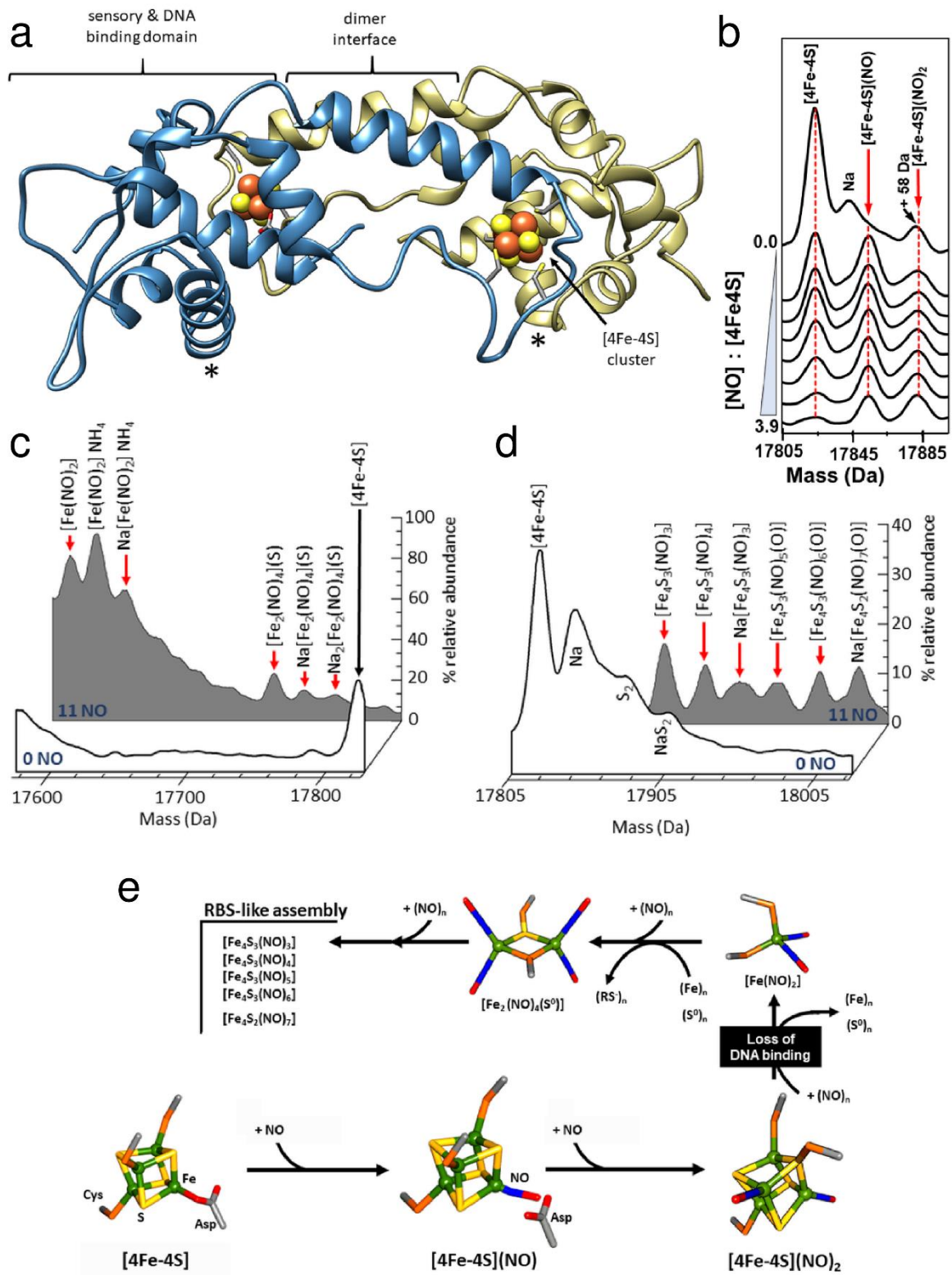


Figure 4

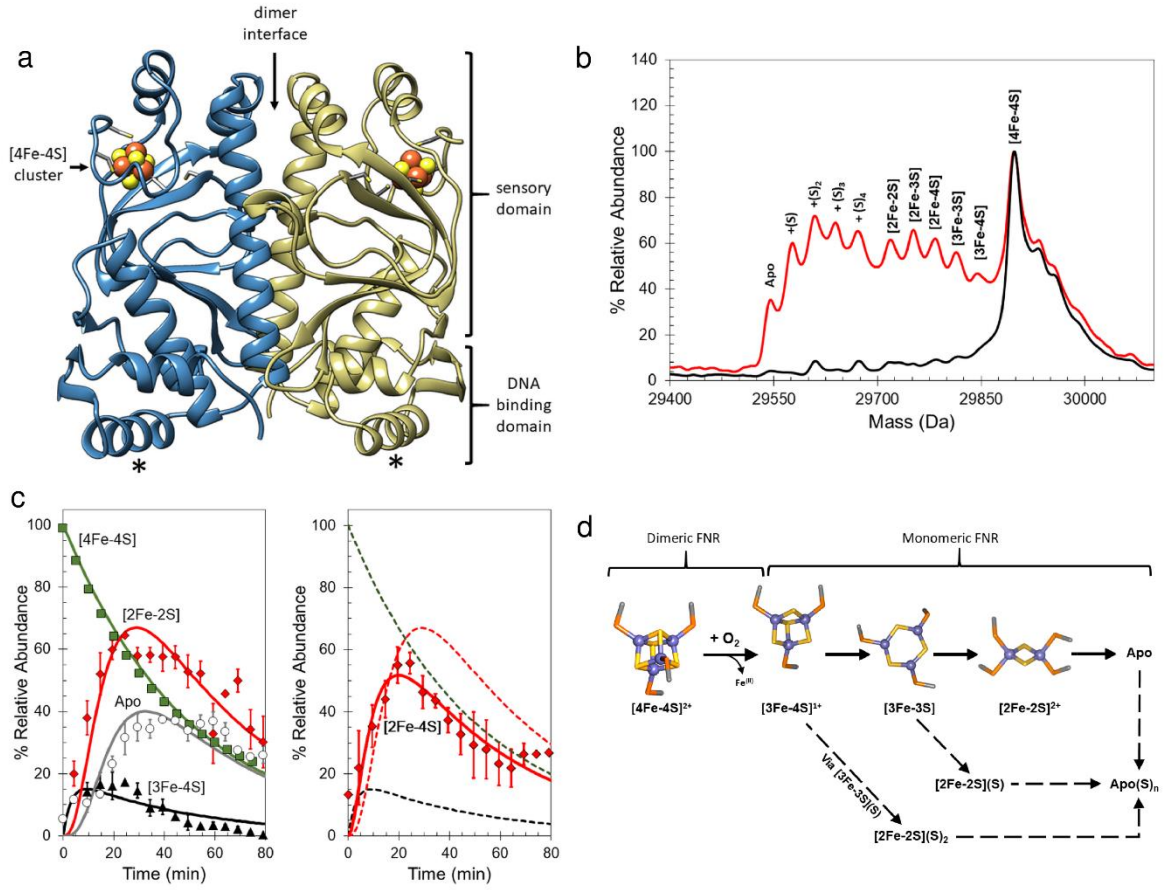


Figure 5